(Received 24 April 2024, Accepted 23 June 2024, Scheduled 2 July 2024)

Non-Conformal Design and Fabrications of Single Arm Conical Log Spiral Antenna

Purno Ghosh[1,*], Frances J. Harackiewicz[2], Liton Chandra Paul[3], and Ashish Mahanta[2]

[1] College of Charleston, SC, USA
[2] Southern Illinois University, Carbondale, IL, USA
[3] Pabna University of Science and Technology, Bangladesh

ABSTRACT: For a conical log spiral antenna (CLSA), it is quite common to place the strip conductor conformally to the conical surface, and the antenna requires an extra impedance matching network. On the other hand, non-conformal orientation can solve the impedance matching issue, but fabrication is not as straightforward as conformal placement. This work considers the non-conformal placement of a strip conductor which facilitates self-matching while using smart additive manufacturing techniques for prototyping to ease the fabrication complexity. The impact of the additional dielectric support on the performance parameters of CLSA is investigated. Finally, the CLSA was prototyped using two different conductive elements (copper strip and conductive paint) on the 3D-printed support. Experimental and numerical results are shown to agree well for both copper strip and paint-based approaches. The self-matched CLSA provided a maximum impedance bandwidth of 128%, 3-dB axial ratio bandwidth (AR BW) of 63.56%, and gains of 10.32 ± 1.94 dBi. The additive manufacturing techniques are shown to allow design flexibility and mitigate fabrication difficulties.

1. INTRODUCTION

Among broadband antennas, the conical log-spiral antenna is one of the most important frequency-independent antennas for producing circular polarization in a wide frequency range and has applications in satellite communications. As stated in [1], two basic methods of angle principle and truncation principle are usually used for designing this type of antenna to make it frequency independent. Truncation principle is taken into consideration in this work which says that the antenna must have a finite active region involved in radiation at any frequency.

Studies have already been done on double-arm conical spiral antenna (CSA). A two-armed CSA in [2] was designed with additional resistors and a balun for a global satellite navigation system where the analysis was limited to simulation only. Two-armed CLSA, quadrifilar helix, and monofilar helix with extra feeding networks were reported in [3–5] for CubeSat applications. An origami design of variable radii helix antenna was demonstrated in [6]. A CSA with two arms including a balun was constructed in [7] with a limited frequency range of 1.9 to 2.1 GHz where the construction was completed on a rolled paper. A wideband compact conical helix was designed in [8] with the non-conformal placement of a strip, but fabrication of the antenna was not reported. An inkjet printable configurable spiral antenna was constructed in [9] where it was shown that the antenna could also be used as a conical spiral, although the spiral alignment was not uniform when being converted to a conical helix. For far-field pattern symmetry, a combination of planar and conical spiral configuration was proposed in [10] without prototyping. Helical antennas including conformal and non-conformal strip orientations have been discussed here [11, 12] but lacking stable fabrication methods. For the above-referenced CSA or CLSA, except [8], the strip conductor was placed conformally relative to the conical surface and used temporary supports for fabrication. Also, an impedance matching section/network is always needed. The fabrication of various types of antennas using additive manufacturing have been discussed in [13, 14] but almost no work on strip-based conical/helical antennas. Here, the fabrication of a strip-based conical antenna is now considered utilizing the advantages of additive manufacturing. Recently, this technique has been used for the fabrications of wire and strip-based spherical, helical, semi-ellipsoidal, and hemispherical antennas [15–18].

Inspired by the significantly wider operational bandwidth of a strip monopole [19] compared to a wire monopole for linear polarization, we have opted to use a strip helix in non-conformal orientation instead of the conventional conformal orientation (strip face wrapped along the conical surface). In this work on CLSA, a single conducting arm is considered and placed in a non-conformal way on the conical surface. Due to this orientation of the conducting strip, the first half turn of the arm at the feed end is almost parallel to the ground plane. The impedance is matched throughout the designed frequency ranges and beyond without using a balun or transformer. Moreover, to ensure the fabrication process is easy and rapid, and smart additive manufacturing is used to build a support structure. This structure helps to maintain the proper alignment and uniform width variation of the strip and the desired spacing between turns for achieving the best performance. The support also provides better mechanical stability and durability over the

* Corresponding author: Purno Ghosh (purnomohon@gmail.com).

paper and foam-based support of other works. Two versions were fabricated, one with flat copper strips and the other with conductive paint.

2. GEOMETRY OF CLSA AND DESIGN EQUATIONS

The conventional geometry and cross-section of a truncated CLSA are shown in Figures 1(a) and 1(b) where a conductive strip is placed conformally to the surface of the cone. The wrap angle (α), half cone angle (θ_0), and upper and lower radii (r_u and r_L) define the complete geometry of the CLSA.

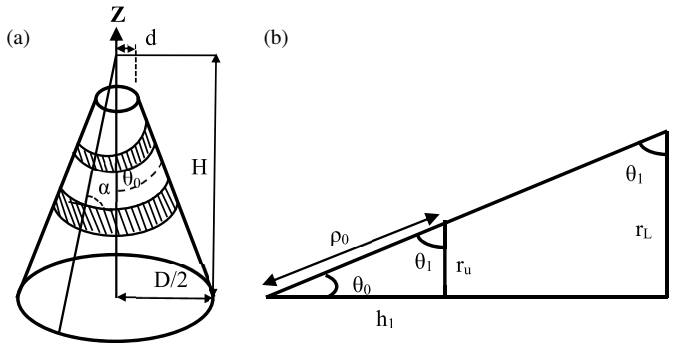

FIGURE 1. (a) Geometry and (b) cross-section of CLSA.

Experimental data from Dyson's study [20] are used in this work to design the single-arm CLSA. The designed frequencies are from 1.8 GHz to 2.7 GHz, and $\lambda_L = 166.55$ mm and $\lambda_u = 111$ mm are corresponding free-space wavelengths at the lower and upper frequencies in the range.

By considering the conical angle $2\theta_0 = 15°$ and wrap angle $\alpha = 80°$, the upper (r_u) and lower (r_L) radii of the truncated cone are calculated from the experimental data of [20] as follows:

$$r_u = 0.083\lambda_u = 9.21\,\text{mm} \quad \text{and} \quad r_L = 0.151\lambda_L = 25.15\,\text{mm}$$

Since the CLSA is a modification of an equiangular spiral, it can be represented [20] by

$$\rho = \rho_0 e^{b\varphi} \ldots \tag{1}$$

where $b = \frac{\sin(\theta_0)}{\tan(\alpha)}$ and $\varphi = 0$ to $\varphi_{\max}$.

From Figure 1(b), $\rho_0 = \frac{r_u}{\sin\theta_0}$ and $h_1 = \rho_0 \sin(90° - \theta_0)$. Using the above relations, $\rho_0 = 70.56$ mm and $h_1 = 69.95$ mm are for this presented work.

The complete height of the cone from the apex is $H = \frac{r_L}{\tan(\theta_0)} = 191$ mm.

The final height of the truncated cone is $h = H - h_1 = 121.10$ mm.

CST Microwave Studio is used for all simulation analysis including the design of the supportive structure. 'Analytical Curve and Face' tools in CST are used to create the strip-based spiral arm. Due to the varying width of the strip, the top and bottom widths of the spiral arm are different. The strip width at the bottom end (feed end) of the CLSA is indicated by W_b and is varied in simulation. At the top of the truncated cone, the strip width is 36.55% of W_b and follows the same relation as $r_u = 36.55\%$ of r_L.

3. SIMULATION ANALYSIS

Simulation analysis is conducted in two steps. In the first step, the strip-based designs (non-conformal orientation of the strip) are considered and shown in Figure 2. In the second step, these better-performing CLSAs are compared with the traditional orientation (conformal) of the conducting strip and analyzed again with the Polylactic Acid (PLA) material-based supportive structure and are shown in Figure 4.

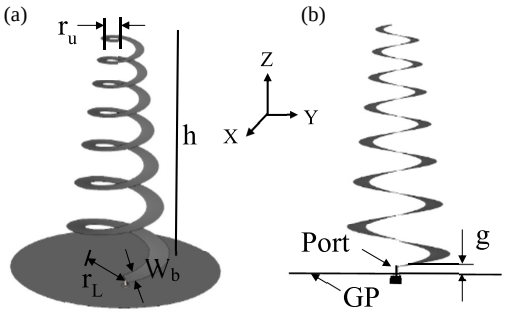

FIGURE 2. Strip-based CLSA. (a) Non-conformal orientation of the strip, (b) front view. GP meant ground plane. r_u and r_L are upper and lower radii. W_b is the strip width at bottom end. 'g' is the gap between GP and strip.

3.1. Impacts of Strip Widths on Reflection Coefficient (S_{11}), AR and Gain

The input impedance of the CLSA is controlled by varying the strip widths. The reflection coefficient (S_{11}) is observed for the strip based CLSA with varying widths ($W_b = 3$ mm to 15 mm) of the strip. It is seen from Figure 3(a) that S_{11} improves (moving towards more negative values) significantly with increasing strip widths. For the strip widths (W_b) of 3 mm and 6 mm, the S_{11} is above -10 dB in the designed frequency range of 1.8 GHz to 2.7 GHz. Further increase of strip widths ($W_b = 9$ mm to 15 mm) significantly improves the impedance bandwidth where the $S_{11} \leq -10$ dB is not limited to the designed frequency range and covers a larger bandwidth. The maximum impedance bandwidth ($S_{11} \leq -10$ dB) of 147% (1.74 GHz to 11.45 GHz) is achieved when $W_b = 12$ mm. There are two factors responsible for the self-matched CLSA with wider impedance bandwidth. They are the use of wide strips with their placement in non-conformal orientation and maintain the bottom end of the strip face as close as possible to the ground plane. The value of the axial ratio (AR) is an indicator of circular polarization (CP). For the ideal case, AR should be 0 dB, but AR $\leq$ 3 dB of any antenna can be considered to judge the ability to produce CP. It is noticed from Figure 3(b) that 3-dB AR bandwidth (BW) almost remains the same with increasing strip widths, and frequencies move toward the expected lower frequency in the designed range. Since the lower frequency of the designed range is 1.8 GHz, $W_b = 12$ mm provided the optimum 3-dB AR BW of 63.52% (2.03 GHz to 3.92 GHz). Throughout the designed frequency range (1.8 GHz to 2.7 GHz), gains increased with increasing strip widths except for the case when $W_b = 15$ mm and are shown in Figure 3(c). For $W_b = 15$ mm, initially gain val-

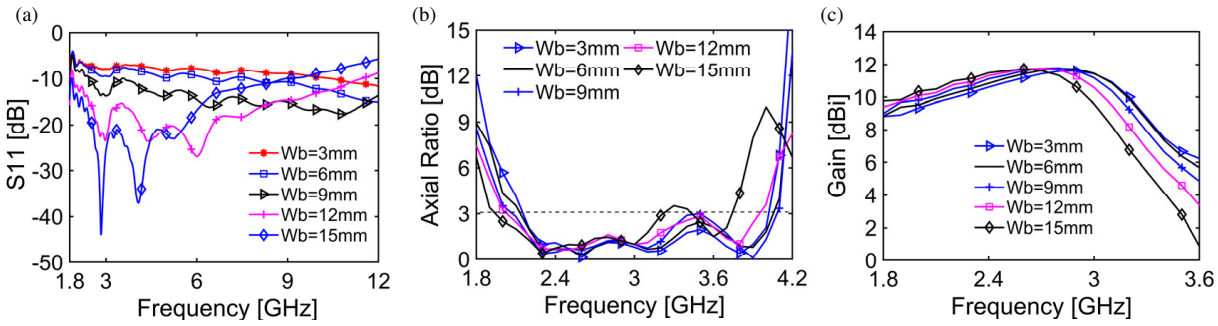

FIGURE 3. Performance comparison of wire and strip-based CLSA. Impacts of variation of strip widths (W_b) on (a) reflection coefficient (S_{11}), (b) axial ratio, and (c) gain.

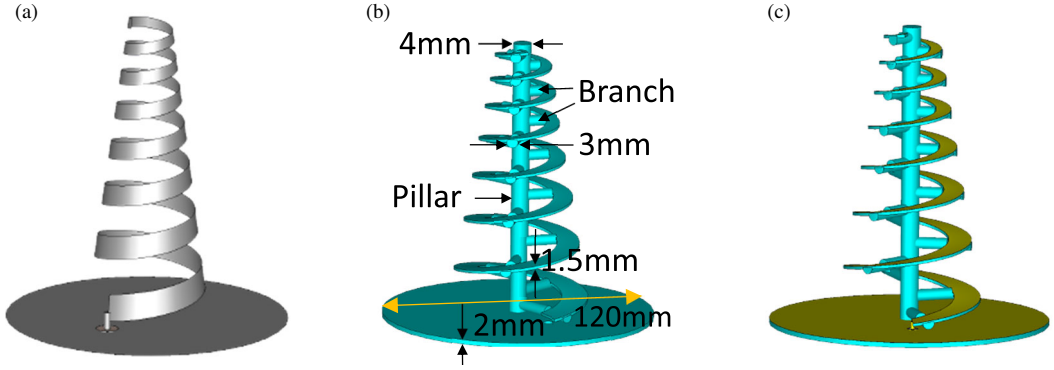

FIGURE 4. (a) Traditional strip orientation, (b) supportive structure with dimensions, and (c) proposed CLSA with support.

ues started to increase but then rapidly go down without maintaining steady growth up to the end frequency in the designed range. For the minimum strip width ($W_b = 3$ mm), the gain variation of 10.12 ± 1.3 dBi is observed. On the other hand, for maximum strip width ($W_b = 15$ mm) the gain variation is 10.64 ± 0.97 dBi. So, gain performances improved with strip widths. Based on the above analysis of impedance bandwidth, AR, and Gain, CLSA provides better performance for the strip width of 12 mm which is considered optimum.

3.2. Impacts of Strip Orientation and Supportive Structure on the Performance of CLSA

The strip-based CLSA of $W_b = 12$ mm is again analyzed with a supportive structure, and its impact on antenna performance parameters is observed. In the same way, the performance parameters of the proposed non-conformal strip orientation are compared with the traditional conformal orientation. Figure 4(a) shows the pictures of CLSA with the traditional orientation of the strip, and the CLSA of proposed non-conformal orientation of the strip is shown early in Figure 2(a). The supportive structure is designed in a way so that it can hold the tapered spiral arm with perfect orientation and alignment. To do so, a central pillar with branches is designed on a circular base which is later used as support for ground planes. The complete supportive structure with dimensional parameters is shown in Figure 4(b). The electrical properties of the material are considered as 3.11 (dielectric constant) and 0.013 (loss tangent), respectively. The proposed CLSA including support is shown in Figure 4(c). It is seen from Figure 5(a) that under the same design parameters, traditional strip orientation (conformal) shows S_{11} of above -10 dB. It is because the wide face of the strip is perpendicular to the ground plane, and the very narrow side is parallel to the ground plane. The narrow side of the strip acts like a thin wire which is the main reason for not obtaining impedance matching under conformal placement. For the impedance matching of wire-based helix type antennas, researchers used a thin but an extra wide metallic strip at the bottom end of the first half turn of helix. This type of additional attachment of strip which was parallel to the ground plane helped to obtain proper matching. On the other hand, the proposed non-conformal strip orientation always maintains $S_{11} \leq -10$ dB. It is seen that after adding the supportive structure, there is no change in impedance bandwidth from the strip-only case, except changes in S_{11} values. The AR BW and gains are also compared among two different strip orientations and strip with supportive structure. It is seen from Figure 5(b) that CLSA with the proposed orientation of the strip provides an improved (63.52%) 3-dB AR BW compared with the traditional orientation (44.36%). The reflection of the travelling current from the open end (not feed end) of the strip has impacts on circular polarization. As the current reflected from the top end more, the AR BW deteriorates which happens for the case of strip with conformal orientation. Including the supportive structure, the obtained 3-dB AR BW is 61% (1.95 GHz to 3.66 GHz) which is 4% less than its strip-only case. Throughout the designed frequency range, the proposed strip orientation also provides an improved gain (10.64 ± 0.97 dBi) compared

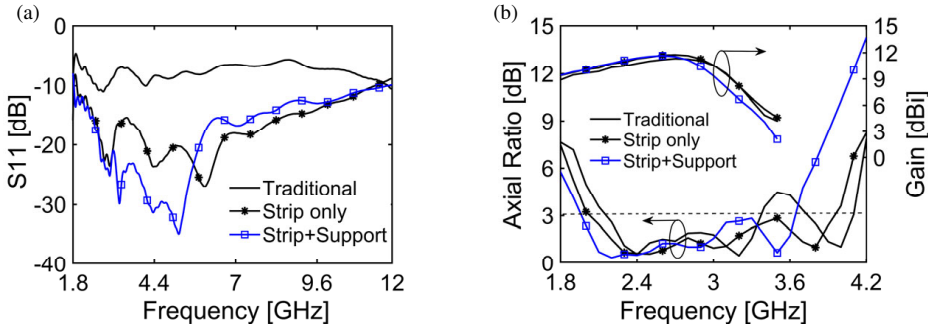

FIGURE 5. Effect of strip orientations and support structure on (a) reflection coefficient (S_{11}), (b) axial ratio and gain.

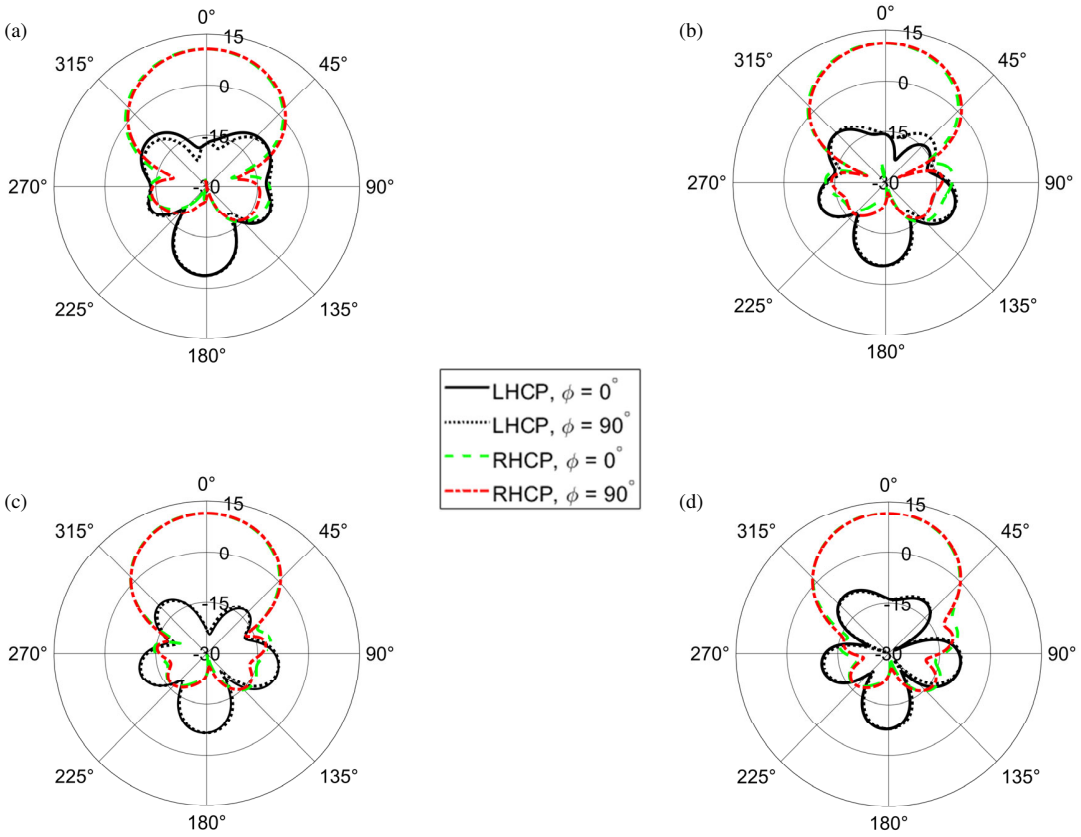

FIGURE 6. LHCP and RHCP elevation gain patterns of the proposed CLSA including support. (a) 2 GHz, (b) 2.2 GHz, (c) 2.4 GHz, (d) 2.6 GHz. Polar and radial axes unit are expressed in degree (°) and dB, respectively.

with the gain (10.11 ± 1.22 dBi) of traditional conformal orientation and is shown in Figure 5(b). Up to 2.6 GHz, gain values are the same for strip and strip-with-support, but after that gain starts to decrease from the strip-only case. At high frequency, the loss properties of the supportive material are responsible for this change. The gain is 10.48 ± 1 dBi including the effect of the support, and it is remarkably close to the gain of the strip-only case.

Figure 6 illustrates the simulated elevation gain patterns for LHCP (left hand circular polarization) and RHCP (Right hand circular polarization) of the antenna at different frequencies of 2 GHz, 2.2 GHz, 2.4 GHz, and 2.6 GHz. The figure indicates that the antenna's right-handed elevation gain is above 10.50 dB when $\theta = 0°$. Additionally, there is at least 25 dB of gain suppression for left-handed circular polarization at the zenith. The proposed CLSA demonstrates exceptional right-handed circularly polarized performance in the designed frequency band.

The efficiency of the CLSA is presented in Figure 7. Dielectric support structure does not have any considerable influence on efficiency. For both cases (strip, and strip with support) the obtained efficiency is above 98%.

3.3. Impacts of Dielectric Constant (ε) of the Supportive Structure

The effects of the dielectric constant (ε) of the supportive material on CLSA performance have been numerically analyzed. It

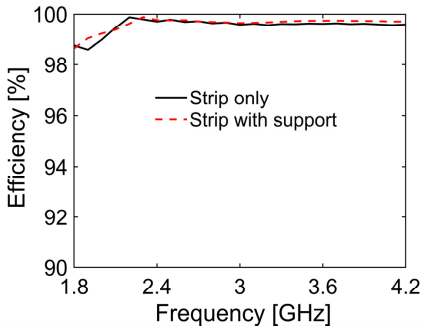

FIGURE 7. Efficiency comparison between two cases (strip only and strip with support) of CLSA.

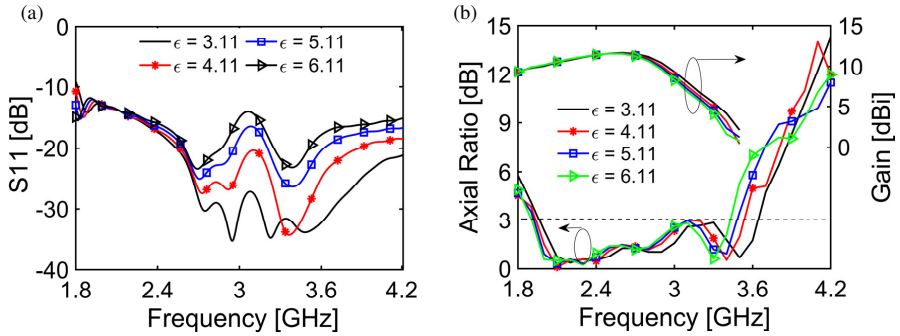

FIGURE 8. Effect of dielectric constant (ε) of the support material on performance of CLSA (a) reflection coefficient (S_{11}), (b) axial ratio and gain.

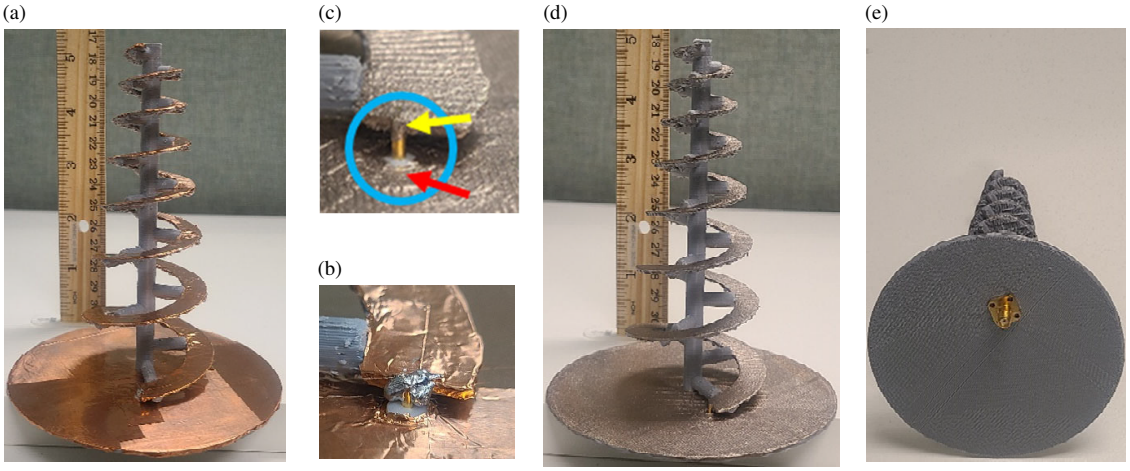

FIGURE 9. Fabricated CLSA. (a) Copper strip-based, (b), (c) coaxial ports, (d) paint-based, (e) connector glued at the backside of the base.

is seen from Figure 8(a) that the magnitude of reflection coefficient (S_{11}) decreases with the increase of dielectric constant but always $S_{11} < -10$ dB for the considered values of ε and frequency range. It is observed from Figure 8(b) that with the increase of dielectric constant, there is a small decrease of AR BW. As shown in Figure 8(b), the gain performance remains almost constant throughout the designed frequency range. After 2.75 GHz, the gain decreases with the increase of dielectric constant.

4. FABRICATION AND EXPERIMENTAL RESULTS

After 3D printing of the PLA material-based supportive structure, it was cleaned and smoothed where isopropyl alcohol and sandpaper were used. As a first metallization approach, the copper tape is used onto the top surface of the spiral arm and circular ground planes of the 3D printed support structure. The conductive strip-based CLSA is shown in Figure 9(a). Among variety of SubMiniature version A (SMA) connectors, a special type was chosen to make the suitable connection with the top surface of circular ground plane. The specialty of this SMA is that its body (external part) has an extra length which forms a cylindrical cup. This extra cup-like shape facilitates penetrating from the bottom of the circular base to the top surface of the ground plane. The core (central lid) of the coaxial connector is soldered to the bottom end of the spiral arm of the copper strip, and the cylindrical body is with the circular ground plane (Figure 9(b)). As a second metallization approach, conductive paint is used for the metallization of the top surface of the 3D printed spiral arm and the circular base. A ready to use MG Chemicals 843WB Super Shield Water Based Silver Coated Copper paint was used to confirm the conductive area. Decent quality paint brushes with round and fine tips are used for painting. Magnifying glass was used to find out if there is any missing paint and significant roughness of the painted surface.

No soldering was applied to paint-based CLSA. Due to the sticky nature of the conductive paint and its capability of drying quickly and thereby turning into solid, paint also helped to secure electrical connection. So, instead of soldering, the same conductive paint is used to attach the central core of the SMA connector with the bottom end of the painted spiral arm, and similarly for the cylindrical body with the painted ground plane (Figure 9(c)). It took an hour from painting to drying to making electrical connection. The paint-based constructed single-arm CLSA is finally shown in Figure 9(d). For both approaches, the flange of the SMA connector is fixed by the adhesive glue at the backside of the supportive base for the rigidity of the connection (Figure 9(e)). S_{11} (dB) magnitude values were measured using Agilent E8362C PNA.

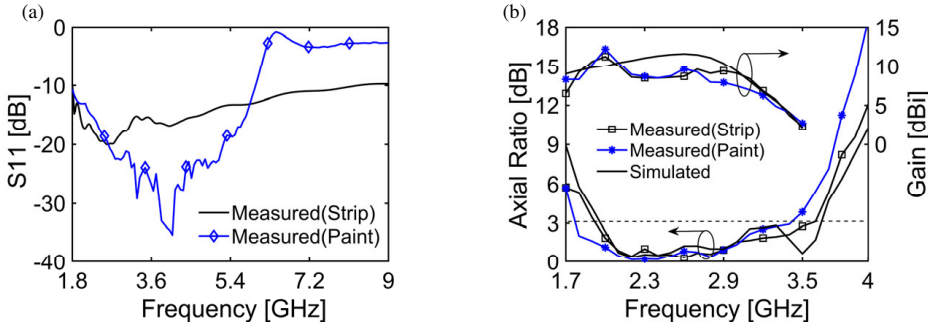

FIGURE 10. Measured results compared with simulation. (a) Reflection coefficient (S_{11}), (b) axial ratio and gain.

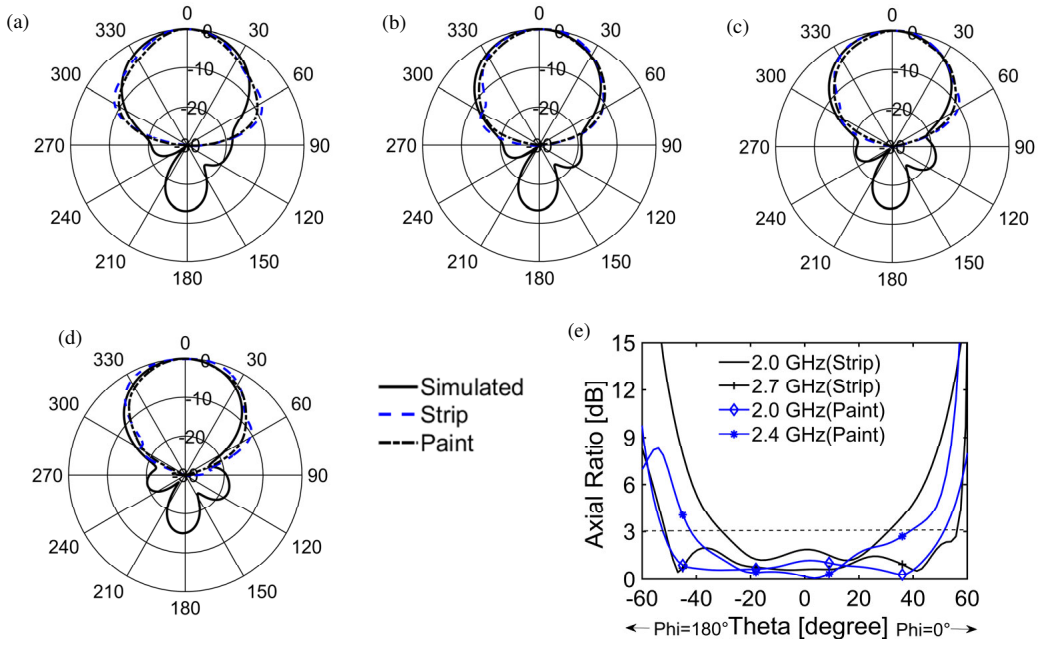

FIGURE 11. Measured radiation patterns at XZ plane ($\phi = 0°$) and beamwidth. (a) 2 GHz, (b) 2.2 GHz, (c) 2.4 GHz, (d) 2.6 GHz. Polar and radial axes unit are expressed in degree (°) and dB, respectively. (e) Minimum and maximum beamwidths of strip and paint-based CLSA.

It is seen from Figure 10(a) that the measured S_{11} for both copper strip and paint-based approaches are well below -10 dB throughout the designed frequency range. The measured impedance bandwidths for the strip and paint-based methods are 128% (1.8 GHz to 8.30 GHz) and 93% (1.8 GHz to 5.95 GHz), respectively. There is good harmony observed between measured and simulated AR values for both strip and paint-based approaches as shown in Figure 10(b). Under the condition of AR $\leq$ 3 dB, the paint-based CLSA covered the lower frequency (1.8 GHz) of the designed range, and the obtained AR BW is 63.56% (1.76 GHz to 3.4 GHz). In an analogous way, for the strip-based method, AR BW is 60% (1.93 GHz to 3.58 GHz). It is seen from Figure 10(b) that there are a few discrepancies in gains between measured and simulated results which resulted in the degradation of the measured gain. This reduction of the gain is due to the more loss properties of the 3D printed material (PLA) at high frequencies. The measured gains for conductive strip and paint-based approaches are 9.90 ± 1.42 dBi and 10.32 ± 1.94 dBi, respectively.

The far-field radiation patterns of CLSA are measured in an anechoic chamber. Radiation patterns of simulated and measured results at four different frequencies throughout the designed frequency range are shown in Figures 11(a)–(d). There is close agreement between the patterns of the strip and paint-based approaches. Measured patterns are also compared with simulated results which are also in good agreement with a little discrepancy. Physical deviations in the antenna construction from the design specifications can lead to differences in performance of the radiation pattern. Small variations in dimensions (irregular sides of the copper tape and infringement of the conductive paint in the undesired area), material properties (loss properties of the support materials and conductivity of the paint), and assembly (adding of SMA with support structure) can impact the radiation pattern. Also, misalignment or improper positioning of the antenna during measurement can affect the radiation pattern. No sidelobes were observed in the measured results, and the back lobes below -30 dB are not shown in the figures. It is also noticed that there is a shifting of the beam from the axial direction ($\theta = 0°$) at a higher frequency

TABLE 1. Comparison with related works.

Ref.		Impedance Bandwidth (%), Self-matched?	3-dB AR BW (%)	Gain (dBi)	Support materials	Base diameter × height (λ_0)
[3] 2-Arms		34, No	31	9 ± 1.5	Foam	0.47×1.04
[7] 2-Arms		10, No	–	4	Paper	0.59×1.06
[8] 1-Arm		81, Yes	58	9 ± 1	No fabrication	0.45×0.45
This work (1-Arm)	**Cu-strip**	**128, Yes**	**60**	$\mathbf{9.90 \pm 1.42}$	**PLA**	$\mathbf{0.38 \times 0.91}$
	Paint	**93, Yes**	**63.56**	$\mathbf{10.32 \pm 1.94}$		

in the designed frequency range, and the maximum beam deviation of 4° is observed at the end frequency of 2.7 GHz. The measured minimum and maximum 3-dB AR beamwidths in the XZ plane ($\phi = 0°$, 180°) for both approaches are shown in Figure 11(e). The minimum and maximum beamwidths covered by the proposed strip-based CLSA are 57° and 94° respectively throughout the designed frequency range of 1.8 GHz to 2.7 GHz. For the paint-based approach, these beamwidths are 72° and 102°, respectively. Table 1 shows a comparison of this presented work with other conical antennas.

5. CONCLUSION

Additive manufacturing technique was brilliantly applied to the quick fabrication of a strip-based conical log-spiral antenna. This fabrication technique provides design flexibility and eases the fabrication complexity of this complexly shaped antenna. The experimental result confirms that the non-conformal deployment of the conductive strip makes the CLSA self-matched, and other performance parameters are comparable to or better than the conformal placement. Conductive paint-based CLSA shows similar performance as the metallic strip-based approach. Finally, under perfect impedance matching condition, the CLSA with proposed strip orientations provides maximum AR BW of 63.56% with a gain of 12.26 dBi. Where needed, future work can consider improving gain performance by using a low-loss material and reducing the percentage fill of the supportive structure.

REFERENCES

[1] Hertel, T. W. and G. S. Smith, "Analysis and design of two-arm conical spiral antennas," *IEEE Transactions on Electromagnetic Compatibility*, Vol. 44, No. 1, 25–37, 2002.

[2] Wei, T. and T. Xiong, "Minimized conical spiral antenna for GNSS," in *2013 IEEE International Conference on Signal Processing, Communication and Computing (ICSPCC 2013)*, 1–4, 2013.

[3] Ernest, A. J., Y. Tawk, J. Costantine, and C. G. Christodoulou, "A bottom fed deployable conical log spiral antenna design for CubeSat," *IEEE Transactions on Antennas and Propagation*, Vol. 63, No. 1, 41–47, 2015.

[4] Costantine, J., Y. Tawk, I. Maqueda, M. Sakovsky, G. Olson, S. Pellegrino, and C. G. Christodoulou, "UHF deployable helical antennas for CubeSats," *IEEE Transactions on Antennas and Propagation*, Vol. 64, No. 9, 3752–3759, 2016.

[5] Sureda, M., M. Sobrino, O. Millan, A. Aguilella, A. Solanellas, M. Badia, J. F. Munoz-Martin, L. Fernandez, J. A. Ruiz-De-Azua, and A. Camps, "Design and testing of a helix antenna deployment system for a 1U CubeSat," *IEEE Access*, Vol. 9, 66 103–66 114, 2021.

[6] Liu, X., C. L. Zekios, and S. V. Georgakopoulos, "Analysis of a packable and tunable origami multi-radii helical antenna," *IEEE Access*, Vol. 7, 13 003–13 014, 2019.

[7] Hussein, K. F. A., "Conical linear spiral antenna for tracking, telemetry and command of low earth orbit satellites," *Progress In Electromagnetics Research C*, Vol. 29, 97–107, 2012.

[8] Mei, J. N., D. W. Ding, and G. Wang, "Design of compact wideband circularly polarized conical helix," in *International Conference on Computer Information Systems and Industrial Applications*, 139–141, 2015.

[9] Saintsing, C. D., B. S. Cook, and M. M. Tentzeris, "An origami inspired reconfigurable spiral antenna," in *2014 International Design Engineering Technical Conferences and Computers and Information in Engineering Conference*, Vol. 46377, Buffalo, NY, USA, 2014.

[10] Huang, J., H. Zhao, Y. Zhou, W. Wu, and N.-C. Yuan, "Far-field symmetry analysis and improvement of the cavity backed planar spiral antenna," *Progress In Electromagnetics Research C*, Vol. 47, 11–18, 2014.

[11] Tang, X., Y. He, and B. Feng, "Design of a wideband circularly polarized strip-helical antenna with a parasitic patch," *IEEE Access*, Vol. 4, 7728–7735, 2016.

[12] Tang, X., B. Feng, and Y. Long, "The analysis of a wideband strip-helical antenna with 1.1 turns," *International Journal of Antennas and Propagation*, Vol. 2016, No. 1, 5 950 472.1–7, 2016.

[13] Helena, D., A. Ramos, T. Varum, and J. N. Matos, "Antenna design using modern additive manufacturing technology: A review," *IEEE Access*, Vol. 8, 177 064–177 083, 2020.

[14] Ghazali, M. I. M., S. Karuppuswami, A. Kaur, and P. Chahal, "3D printed high functional density packaging compatible out-of-plane antennas," *Additive Manufacturing*, Vol. 30, 100863, 2019.

[15] Ghosh, P. and F. Harackiewicz, "3D printed low profile strip-based helical antenna," *Progress In Electromagnetics Research C*, Vol. 127, 195–205, 2022.

[16] Ghosh, P. and F. J. Harackiewicz, "Three-dimensional-printed strip and paint-based semiellipsoidal helical antenna," *Microwave and Optical Technology Letters*, Vol. 65, No. 8, 2262–2266, 2023.

[17] Ghosh, P. and F. Harackiewicz, "Analysis and fabrication of conductive strip and paint-based hemispherical helical antennas on

3D printed structure," *Progress In Electromagnetics Research C*, Vol. 135, 1–11, 2023.

[18] Ghosh, P., L. C. Paul, and T. Rani, "Rapid construction of electrically small spherical and cylindrical antennas," *e-Prime — Advances in Electrical Engineering, Electronics and Energy*, Vol. 8, 100631, 2024.

[19] Wong, K.-L. and Y.-F. Lin, "Stripline-fed printed triangular monopole," *Electronics Letters*, Vol. 33, No. 17, 1428–1429, 1997.

[20] Dyson, J., "The characteristics and design of the conical log-spiral antenna," *IEEE Transactions on Antennas and Propagation*, Vol. 13, No. 4, 488–499, 1965.